Determination of Spatial Amplification Factors and Their Application to Predicting Transition

N. A. JAFFE,* T. T. OKAMURA,† AND A. M. O. SMITH‡
Douglas Aircraft Company, Long Beach, Calif.

A method for applying stability theory to the problem of predicting transition is described. The Orr-Sommerfeld equation is employed to perform a stability analysis on laminar boundary-layer velocity profiles that have been obtained numerically for two-dimensional and axisymmetric flows. An orthogonalization technique capable of handling Reynolds numbers, based on displacement thickness, up to at least the order of 10^5 is used to obtain spatial amplification rates of small disturbances over a select frequency band at various streamwise locations. For each of the frequencies considered the amplification rate is integrated with respect to surface distance downstream from the point of neutral stability in order to obtain an amplification factor. The disturbance whose frequency produces a maximum amplification factor at transition is considered for correlation purposes. A partial examination of currently available data from low freestream turbulence tests revealed a good correlation between the observed location of transition and a maximum amplification factor of the order of e^{10}.

Nomenclature

a = amplification factor, ratio of amplitude of a disturbance to its amplitude at neutral stability
c = complex velocity of Tollmien-Schlichting wave, nondimensionalized with respect to u_e
L = characteristic length, chord for airfoil
R = local Reynolds number based on boundary-layer thickness, $u_e\delta/\nu$
R_L = freestream Reynolds number based on chord length, $u_\infty L/\nu$
R_x = local Reynolds number based on surface distance x_* from leading edge, $u_e x_*/\nu$
$R_{\delta*}$ = local Reynolds number based on displacement thickness, $u_e\delta^*/\nu$
u = streamwise velocity component
U = dimensionless streamwise velocity component, u/u_e
x = distance along surface, nondimensionalized with respect to boundary-layer thickness, x_*/δ
y = distance normal to surface nondimensionalized with respect to boundary-layer thickness, y_*/δ
X = distance along surface nondimensionalized with respect to chord length, x_*/L
α = complex eigenvalue $\alpha_r + i\alpha_i$
α_i = spatial amplification rate, nondimensionalized with respect to boundary-layer thickness, $\alpha_{i*}\delta$
α_r = wave number, nondimensionalized with respect to boundary-layer thickness, $\alpha_{r*}\delta$
δ = boundary-layer thickness, where $U = 0.999$ in present investigation
δ^* = displacement thickness
Δ = Laplace operator
φ = disturbance amplitude
Φ = particular eigenfunction solution (linear combination of φ's)
ψ = disturbance stream function
ψ_0 = mean flow stream function
Ψ = total stream function
ν = kinematic viscosity
ζ = vorticity
ω = dimensionless frequency, $\omega_*\nu/u_e^2$

Subscripts

e = edge of boundary layer
i = imaginary part of complex quantity
m = maximum value of function, i.e., a_m
n = location of neutral stability
r = real part of complex quantity
tr = location of transition
w = wall
$*$ = dimensional quantities indicated by $(\ )_*$
∞ = freestream

Presented as Paper 69-10 at the AIAA 7th Aerospace Sciences Meeting, New York, January 20–22, 1969; submitted February 3, 1969; revision received June 30, 1969. Also Douglas Paper 5504.

* Senior Engineer/Scientist, Aerodynamics Research. Associate Fellow AIAA.
† Engineer Scientist/Specialist, Aerodynamics Research.
‡ Chief Aerodynamics Engineer, Research. Fellow AIAA.

1. Introduction

THIS paper presents the results of an application of stability theory to the problem of locating boundary-layer transition on axisymmetric or two-dimensional bodies having arbitrary pressure distributions in incompressible flow. Disturbances in the boundary layer that grow at the rate predicted by the Orr-Sommerfeld (O-S) equation are considered.

Wave solutions satisfying the O-S equation were obtained by Tollmien and Schlichting[1] before such waves were experimentally observed. In the process of reducing turbulence levels to very low values for transition studies on a flat plate, Schubauer and Skramstad[2] observed such waves. Apparently high turbulence levels in previous investigations had obscured them. Subsequently Bennett,[3] using more sophisticated techniques, observed Tollmien-Schlichting waves in a tunnel whose turbulence level was as high as $u'/U_\infty = 0.42\%$; the turbulence level in the experiments of Schubauer and Skramstad had been reduced to 0.05%. Since these waves have been observed under conditions of low and intermediate turbulence levels and since in-flight turbulence levels are very low, they may have bearing on the transition process taking place in free flight.

The connection between stability theory and transition is still largely unresolved; however, a semiempirical method based on stability theory for predicting transition, developed independently by Smith[4] and Van Ingen,[5] enjoyed a large degree of success. The analysis in Refs. 4 and 5 was based on the application of Pretsch's[6] charts for the stability characteristics of Falkner-Skan profiles having temporal disturbances. However, the observed disturbances in the experiments of Schubauer and Skramstad[2] and more recently Klebanoff, Tidstrom, and Sargent[7] indicate transition arising from the growth of spatial disturbances, and it is with the

nature of this type of disturbance that the present investigation is concerned.

Various alternatives exist for bridging the gap between temporal and spatial analyses. In Refs. 4 and 5 the phase velocity c_r obtained from a temporal analysis is used to obtain the spatial growth rate by employing the following expression for the distance the disturbance travels over a given time interval:

$$dx = c_r dt$$

The foregoing is approximate since the group velocity c_g should be employed rather than the phase velocity. By neglecting terms of order c_i^2 in comparison to $\alpha c_i/c_g$, where α in the temporal analysis is taken to be real and αc the frequency is imaginary, Gaster[8] derives the following relation between group and phase velocity:

$$c_g = c_r + \alpha(\partial c_r/\partial\alpha) = (\partial\omega_r/\partial\alpha_r)$$

In the present analysis αc is restricted to real values initially and the imaginary part of α, α_i automatically yields the spatial growth rate of the disturbance.

In a sense, this study is a re-examination of the concepts applied in Refs. 4 and 5; however, there are the following significant differences: the stability analysis is performed on exact laminar velocity profiles rather than on profiles based on the assumption of similarity, spatial rather than temporal disturbances are considered (the stability characteristics of the two are identical only for the case of neutral stability), and a technique for obtaining more accurate eigenvalues than those given by Pretsch has been employed.

For many years the mathematical difficulties encountered in stability analyses discouraged attempts to improve upon Pretsch's charts. On the one hand, the results obtained by asymptotic analytic methods (applicable to high Reynolds number flows) are severely restricted, and on the other hand, numerical techniques become cumbersome with increasing Reynolds number, thus yielding a large Reynolds number range over which it is difficult to obtain stability data. Advances in the application of numerical techniques have eased this difficulty. Of note is the "purification scheme" of Landahl and Kaplan[9] which can handle Reynolds numbers based upon boundary-layer thickness up to 10^4. A more precise formulation of this procedure, the technique of Gram-Schmidt orthogonalization[10] has been applied by Wazzan, Okamura, and Smith[11,12] and is capable of obtaining stability characteristics of boundary-layer profiles up to Reynolds numbers at least two orders of magnitude greater than previous techniques. This technique has been incorporated in the present study.

Recently Reshotko[13] indicated the possibility of applying stability theory as a guide to obtaining transition correlations with supersonic test data. This work is mainly concerned with the possibility of correlating the location of transition (transition Reynolds number) with the point at which the amplification rate of a given frequency is a maximum. In the present analysis the total integral of the amplification rate from the point of neutral stability up to the transition point is considered for correlation purposes rather than a point value of this quantity. Moreover, disturbance frequencies characteristic of a particular test facility were considered in Ref. 13 whereas in the present investigation the frequency which maximizes the integral of the amplification rate at transition is considered for correlation purposes. The different approaches taken between this investigation and that reported in Ref. 13 are due primarily to the fact that the emphasis in the present study is on obtaining a suitable method for predicting transition under free flight conditions whereas the emphasis in the latter investigation is on correlating wind-tunnel data.

2. Analysis

In the present analysis a powerful numerical technique is employed to obtain solutions to the O-S equation. The stability analysis is performed on laminar velocity profiles that have also been obtained numerically for incompressible flow over two-dimensional or axisymmetric bodies. Dimensionless velocity profiles $[U = U(y_*/\delta)]$ are obtained at various streamwise locations for the body under consideration; it is pointed out that only if the flow is similar will the function $U(y_*/\delta)$ be invariant with position along the body surface.

In order to obtain disturbance amplification rates for a given Reynolds number, the disturbance frequency and local Reynolds number based on boundary-layer thickness must be specified along the surface; the latter quantity is fixed by the freestream unit Reynolds number. Only a finite band of frequencies need be considered since all disturbances with frequencies above a certain level are not amplified and frequencies below a certain level do not begin being amplified until another, higher-frequency disturbance, has already led to transition. If, for example, laminar flow existed over the whole body there would be a lower limit corresponding to that frequency which is not amplified until the trailing edge. Thus, the laminar boundary layer on a finite body can be considered as an amplifier for a select frequency band.

The amplification rates that are obtained from solutions to the O-S equation are integrated for a fixed frequency, with respect to the streamwise coordinate from the point of neutral stability, yielding the natural logarithm of the amplification factor $a(X)$. The amplification factor at a given location past the point of neutral stability represents the ratio of the magnitude of the disturbance at X to its value at the neutral point. At a given location the amplification factor is a function of frequency exhibiting a maximum. The disturbance producing the maximum value of the amplification factor at transition is assumed to be the one that causes transition in the present investigation.

A logical justification for using maximum amplification factors to predict transition has been given by Liepmann.[14] It is suggested in this reference that where the Reynolds shear τ_T first reaches the magnitude of the laminar shear τ_L be taken as the location of transition. This criterion is given by

$$[(\tau_T)_{\max}/\tau_L] = (1/c_{fL})[kb(u'/u_e)_n{}^2 a^2(X)]_{\max}$$

where $b = v'/u'$ (ratio of y fluctuation velocity component to x velocity fluctuation component), c_{fL} = laminar skin-friction coefficient, $k = \overline{u'v'}/uv$ (correlation coefficient).

The preceding expression contains the product of a term representing the turbulence level at the beginning of transition (neutral point) $(u'/u_e)_n$, and a ratio of levels over the transition region $a(X)$. Thus an exact treatment, in order to be consistent with Liepmann's theory, should consider the actual magnitude of the disturbance level for correlation purposes. It is found from experimental data that at transition $a(X)$ is the major variable, which for most cases is the order of at least e^8, in the previously mentioned expression. Therefore, in any first-order correlation study, variations of the other factors are neglected.

2.1 Computation of Amplification Rates

Details of the numerical techniques employed in this investigation to obtain stability data can be found in Refs. 11 and 12; hence only the basic equations and general features of the numerical analysis are given here.

Combining the equations of momentum and continuity for unsteady two-dimensional flow of an incompressible fluid yields the following equation of motion in terms of vorticity

$\zeta(t,x,y)$ and stream function $\Psi(t,x,y)$:

$$\partial\zeta/\partial t = (i/R)\Delta\zeta + (\partial\Psi/\partial x)\partial\zeta/\partial y - (\partial\Psi/\partial y)\partial\zeta/\partial x \quad (1)$$

where

$$\zeta = \Delta\Psi \quad (2)$$

The aforementioned equations have been made dimensionless by normalizing length with respect to δ, the boundary-layer thickness, velocities with respect to u_e and time by δ/u_e. The stream function Ψ is replaced by a mean value ψ_o and a superimposed small disturbance ψ. Assuming the mean stream function satisfies conditions of parallel flow we have

$$\Psi = \psi_0(y) + \psi(x,y,t) \quad (3)$$

Furthermore, it is assumed that the disturbance stream function can be represented by a Fourier series and that the nonlinear disturbance terms can be neglected. A single disturbance mode is given by

$$\psi = \varphi(y)e^{i\alpha(x-ct)} \quad (4)$$

known as a Tollmien-Schlichting wave. Substitution of the quantities given by Eqs. (2–4) into Eq. (1) leads to the Orr-Sommerfeld equation

$$(U - c)(\varphi'' - \alpha^2\varphi) - U''\varphi = -(i/\alpha R)(\varphi'''' - 2\alpha^2\varphi'' + \alpha^4\varphi) \quad (5)$$

where primed quantities are derivatives with respect to y, α is a complex number of which the imaginary part α_i is the disturbance amplification rate and the real part α_r the wave number, and c is a complex number of which the real part c_r is the phase speed. Assuming the disturbance is spatial imposes the restriction that the product αc is real and represents the disturbance frequency ω, $\alpha c = R\omega$ (real). The quantity U is a function representing the dimensionless velocity profile and R the Reynolds number. $u/u_e = U(y)$, $R = u_e\delta/\nu$. The boundary conditions on Eq. (5) are

$$y = 0: \quad \varphi = \varphi' = 0 \quad (6)$$

$$y \to \infty: \quad \varphi = \varphi' = 0 \quad (7)$$

The homogeneous boundary conditions lead to a boundary value problem of the eigenvalue type in turn leading to the solution of a secular equation of the form

$$F(\alpha,\omega,R) = 0 \quad (8)$$

The quantity δ is arbitrarily taken as the distance from the wall at which the velocity is 0.999 of its value ($U = 0.999$) at the edge of the boundary layer. The final results, for convenience, employ R_{δ^*} the Reynolds number based on displacement thickness rather than R as a parameter.

As the edge of the boundary layer is approached $U \to 1$, and Eq. (5) has the following two solutions satisfying the proper boundary conditions as $y \to \infty$:

$$\varphi_1 = \exp(-\alpha y) \quad (9)$$

$$\varphi_2 = \exp\{-(\alpha^2 + i\alpha R[1 - c])^{1/2}y\} \quad (10)$$

These two linearly independent solutions are taken as initial conditions at $y = 1$. Using these two solutions, Eq. (5) is integrated from $y = 1$ towards the surface; at the surface they are combined linearly to satisfy boundary conditions. Round-off errors can lead to a deterioration of the linear independency of φ_1 and φ_2 at large values of R during integration of Eq. (5) from the boundary-layer edge to the wall. This difficulty is circumvented by applying the technique of Gram-Schmidt orthogonalization.[10] Individual solutions are considered as vectors in a function space having components (φ, φ', φ'', φ'''). To insure linear independence at the end of each integration interval, the initial solutions φ_1 and φ_2 are orthogonalized.[11] That is, at the end point of an integration interval y_k, orthonormal solutions $\tilde{\varphi}_1(y_k)$ and $\tilde{\varphi}_2(y_k)$ are constructed from $\varphi_1(y_k)$ and $\varphi_2(y_k)$ using the relations

$$\tilde{\varphi}_2(y_k) = \varphi_2(k)/|\varphi_2(k)| \quad (11)$$

$$\tilde{\varphi}_1(y_k) = \varphi_1(y_k) - [\varphi_1(y_k)\cdot\tilde{\varphi}_2(y_k)]\tilde{\varphi}_2(y_k) \quad (12)$$

The quantities $\tilde{\varphi}_1$ and $\tilde{\varphi}_2$ satisfy the O-S equation and $\tilde{\varphi}_1$ can be considered as purified from any vector component of $\tilde{\varphi}_2$.

Since the solution to Eq. (5) is an eigenvalue problem, specification of the Reynolds number R and frequency ω will yield a solution satisfying the boundary conditions only for properly selected values of α [see Eq. (8)]; thus an iteration procedure is employed to obtain the proper eigenvalues. The functions $\tilde{\varphi}_1$ and $\tilde{\varphi}_2$ are linearly combined at the surface to obtain the eigenvalues. A linear combination Φ that is a solution to Eq. (5) is given by

$$\Phi = \tilde{\varphi}_1 + B\tilde{\varphi}_2 \quad (13)$$

where B is obtained from the requirement that

$$\Phi(0) + K\Phi'(0) = 0 \quad (14)$$

and K is an arbitrary constant. It is pointed out that while exact eigenvalues can be obtained the eigenfunctions can only be obtained to within an arbitrary constant. The absolute turbulence level at the edge or at any specified point within the boundary layer is needed to determine this constant. The condition that the boundary-layer admittance $Z(\alpha,\omega,R)$ vanish is substituted for the condition $\Phi(0) = 0$ where Z is given by

$$Z(\alpha,\omega,R) = -\alpha^2R\Phi(0)/[\Phi'''(0) - \alpha^2\Phi'(0)] \quad (15)$$

and Φ satisfies Eqs. (13) and (14). Thus the problem of satisfying the boundary conditions reduces to that of finding the value of α which causes the admittance to vanish. Since Z and α are complex and ω and R are specified, in functional form, the problem reduces to finding the roots of

$$Z_r = Z_r(\alpha_r,\alpha_i) = 0 \quad (16)$$

$$Z_i = Z_i(\alpha_r,\alpha_i) = 0 \quad (17)$$

Because of the acute sensitivity of the topology of Z to small changes in α, standard iteration techniques proved unsuitable to solve these equations. For example, the use of Lagrange-type interpolation employed by Landahl and Kaplan proved unsatisfactory for the Reynolds number range of interest. The procedure adopted is to fit a plane to three successive trial points of the form

$$Z = a_0 + a_1Z_r + a_2Z_i \quad (18)$$

where the coefficients a are complex. The first two trial points are based on estimates or extrapolations of previously obtained eigenvalues, the third from a linear prediction based on the first two; thereafter Eq. (18) is employed. One free parameter, namely K in Eq. (14), can be employed to modify the topology of the surfaces given by Eqs. (16) and (17). It is found that using a value of $U''(0)/c$ for K is convenient for numerical purposes.

The velocity profiles needed are obtained from numerical solutions to the laminar boundary-layer equations. The form of the partial differential equation solved is given in Ref. 15. The problem of solving the partial differential equation is reduced to that of solving, consecutively, a set of ordinary differential equations by first replacing the streamwise derivatives with a least-square approximation and the ordinary equations which are of the nonlinear boundary value type are then solved using an initial value variational technique.[16]

2.2 Determination of Amplification Factors

Figures 1–3 demonstrate typical computed stability characteristics of velocity profiles corresponding to a favorable

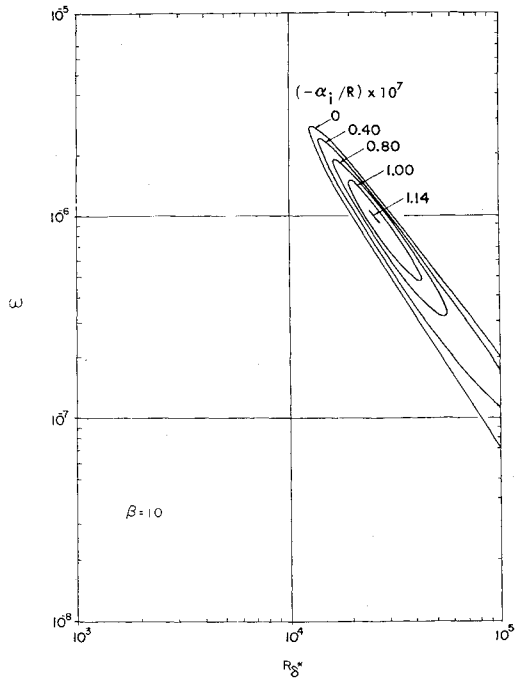

Fig. 1 Stability chart—stagnation point flow.

pressure gradient, zero pressure gradient, and adverse pressure gradient. The profiles used are from solutions to the Falkner-Skan equation for different values of the Hartree parameter β, where $\beta = 1$ for stagnation flow, $\beta = 0$ flat-plate flow, and $\beta = -0.1988$ for separation flow.[12] The disturbance frequency ω is plotted as a function of Reynolds number based on boundary-layer displacement thickness for various values of the normalized dimensionless amplification rate α_i/R where the dimensionless amplification rate α_i is related to the dimensional amplification rate α_{i*} (length)$^{-1}$ through

$$\alpha_i/R = \alpha_{i*}\nu/u_e \tag{19}$$

Only curves for neutral and amplified disturbances ($\alpha_i \leq 0$) are shown. The lower branch of the curve for $\alpha_i = 0$ determines the relation between the frequency and the Reynolds number corresponding to neutral stability. Taking x_* as the dimensional curvilinear coordinate measured along the surface, the total apparent amplification (amplification factor) of a fixed frequency disturbance from the neutral point to some location x_* downstream is given by

$$a = \exp - \int_{x_{*_n}}^{x_*} \alpha_{i_*} dx_* \tag{20}$$

$$\omega_* = (u_e^2/\nu)\omega = \text{const}$$

In terms of dimensionless quantities this expression becomes

$$a(X) = \exp -R_L \int_{X_n}^{X} \left(\frac{\alpha_i}{R}\right)\left(\frac{u_e}{u_\infty}\right) dX \tag{21}$$

$$\omega(u_e/u_\infty)^2 = \text{const}$$

where $X = x_*/L$, $R_L = u_\infty L/\nu$, L = characteristic body length (chord length on airfoil).

It is pointed out that the amplification factor is actually an apparent amplification of a fixed frequency disturbance since the disturbance may not be of the form given by Eq. (4) and in the vicinity of transition the linearized theory may break down.

Thus by specifying the freestream Reynolds number, the variation of u_e/u_∞ with X, and determining the variation of (α_i/R) with X from stability theory the amplification factor at any location and in particular at the point of transition X_{tr} can be evaluated. Stability charts such as shown in Figs. 1–3, strictly speaking, can only be used to obtain amplification factors for similar flows. That is, each of these figures exhibit the stability characteristics of a velocity profile U which is invariant with X; the amplification rate for a fixed frequency varies with X only because the quantity R [see Eq. (5)] varies with X. In general, flows are nonsimilar and the amplification rate varies due to a variation of both U and R with X. In the present analysis a step-by-step calculation is employed marching downstream. At each streamwise location the velocity profile U is first determined numerically and then the amplification rate α_i for the specified value of R at that location, is obtained for each frequency considered. Determination of a complete stability chart for each velocity profile considered is unnecessary since amplification rates over a select frequency band are needed for that profile only for a single Reynolds number in order to obtain amplification factors in any given case.

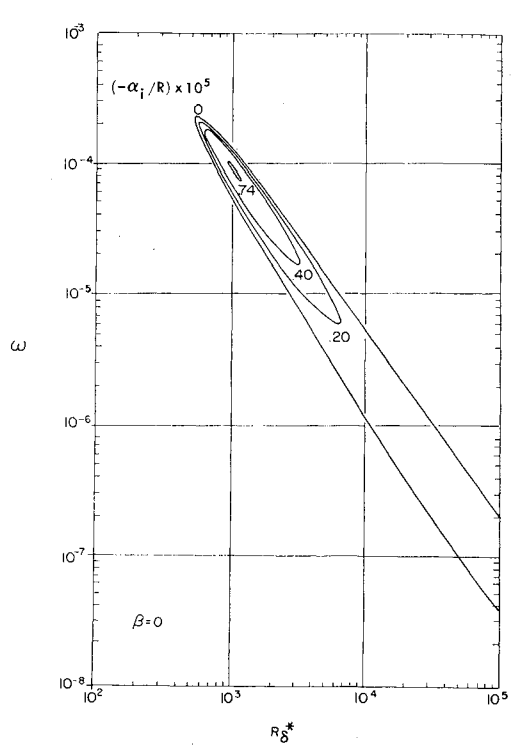

Fig. 2 Stability chart—flat plate flow.

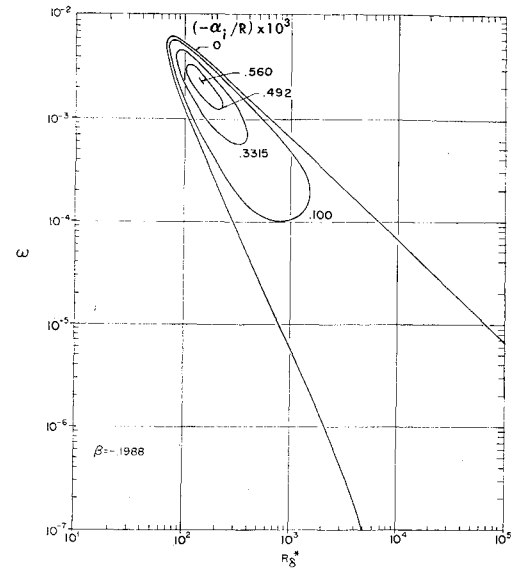

Fig. 3 Stability chart—separating flow.

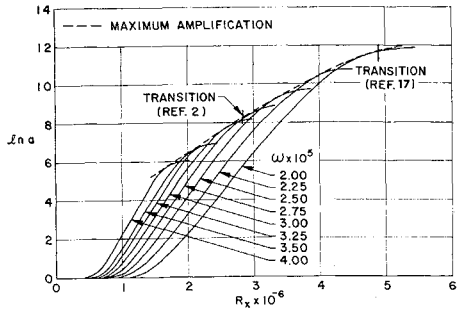

Fig. 4 Amplification factors—flat plate.

As mentioned earlier, the value of $a(X)$ at any particular location will vary with the frequency of the disturbance and exhibit a maximum, a_m; for correlation purposes the maximum value of the amplification factor at transition $a_m(X_{tr})$ will be considered.

3. Results and Discussion

Numerical results are given for axisymmetric and two-dimensional bodies at various freestream Reynolds numbers. The bodies studied are those for which transition data at low freestream turbulence levels is available. Not all of the available data to date has been examined; further studies are being continued, and as new data becomes available it too shall be incorporated in the present analysis. The following bodies were investigated: 1) flat plate, experimental data taken from Refs. 2 and 17; 2) symmetrical airfoil NACA 0012, data from Ref. 18; 3) upper and lower surfaces of NACA 35-215, data from Ref. 19; 4) upper and lower surfaces of NACA $65_{(215)}$-114, data from Ref. 20; 5) axisymmetric body of revolution of fineness ratio 9.0, data from Ref. 21; 6) axisymmetric body of revolution of fineness ratio 10.0, data transmitted by private communication with NPL, England.

Figure 4 shows the variation of the natural logarithm of the computed amplification factors with R_x for flow on a flat plate over a dimensionless frequency band, $\omega_* \nu/u_e^2$, ranging from 2×10^{-5} to 4×10^{-5}. These frequencies were chosen since they produce maximum amplification in the neighborhood of transition. The envelope of these curves represents the maximum amplification factor. The variation of $\ln a$ with frequency at a given location can also be seen. Schubauer and Skramstad[2] observed transition at a value of $R_x = 2.84 \times 10^6$ and subsequently Wells Jr.[15] observed transition at $R_x = 4.9 \times 10^6$ under low freestream turbulence conditions. The higher value of R_x is attributed[17] to careful suppression of acoustical disturbances assumed present in the earlier experiments of Schubauer and Skramstad. The computed values of $\ln a_m$ at the two observed locations of transition are 8.3 and 11.8.

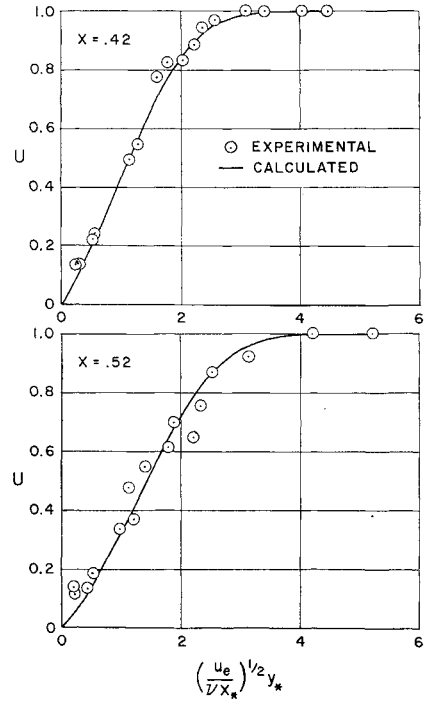

Fig. 5 Velocity profile comparisons—NACA 0012, $C_L = 0$.

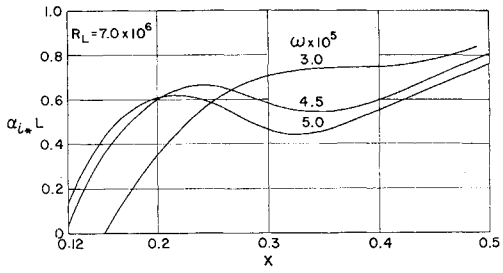

Fig. 6 Amplification rates—NACA 0012, $C_L = 0$.

The laminar velocity profiles for the NACA 0012 airfoil were computed using the experimental pressure distribution given in Ref. 18. Typical examples of comparisons between computed and measured velocity profiles are shown in Fig. 5. The variation of amplification factor with dimensionless surface distance x, (x_*/L), was determined for freestream Reynolds numbers, R_L of 2.5×10^6, 5.0×10^6, and 7.0×10^6; the observed locations of transition, X_{tr}, for these conditions are 0.49, 0.355, and 0.32, respectively. Figure 6 shows a plot of the dimensionless amplification rate [integrand in Eq. (8)] as a function of X beginning at approximately the point of neutral stability ($\alpha_{i*} = 0$) for frequencies in the neighborhood of that producing maximum amplification at transition for the highest freestream Reynolds number ($R_L = 7.0 \times 10^6$) considered. It can be seen from this figure that the amplification rate is not necessarily a monotonic function. The amplification factor (the integral of the amplification rate) is monotonic, however, unless the disturbance is damped after it has once been amplified. Figure 7 shows the variation of amplification factor with X over a band of frequencies at $R_L = 7.0 \times 10^6$; in addition the variation of amplification factor with frequency at transition is shown. Figure 8 shows the variation of the experimentally observed location of transition with freestream Reynolds number and that which would be theoretically predicted based upon the constant amplification factors of e^{11} and e^{12}.

Amplification factors were computed for the upper and lower surfaces of the NACA 35-215 airfoil at a freestream Reynolds number R_L of 26.7×10^6 and lift coefficient of 0.238.[19] Under the most favorable conditions the observed

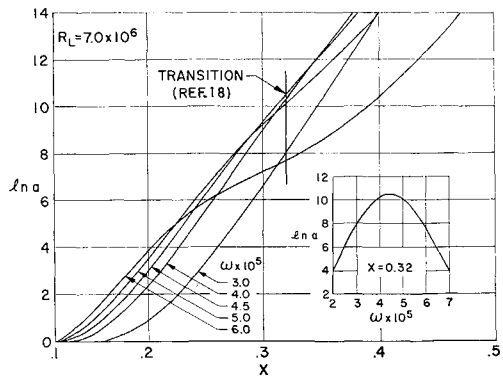

Fig. 7 Amplification factors—NACA 0012, $C_L = 0$.

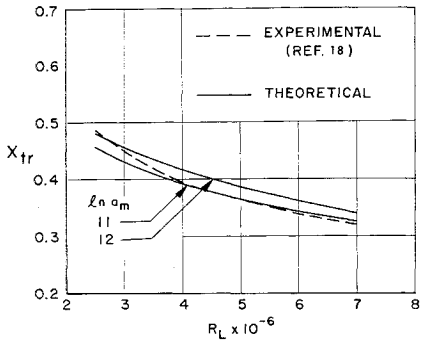

Fig. 8 Predicted and experimental location of transition—NACA 0012, $C_L = 0$.

transition Reynolds numbers, R_x, during flight tests were found to be 15.4×10^6 and 10.2×10^6, corresponding to fractions of chord of 0.45 and 0.30 for upper and lower surfaces, respectively. According to Ref. 19 transition may have been influenced by waviness on the lower surface. The computed values of $\ln a_m$ for the upper and lower surfaces at transition, for the aforementioned conditions, are 9.9 and 9.0, respectively. Figure 9 shows computed amplification factors on the lower surface over a range of frequencies in the neighborhood of that producing maximum amplification.

Amplification factors were obtained for the upper and lower surfaces of the NACA $62_{(215)}$-114 airfoil at freestream

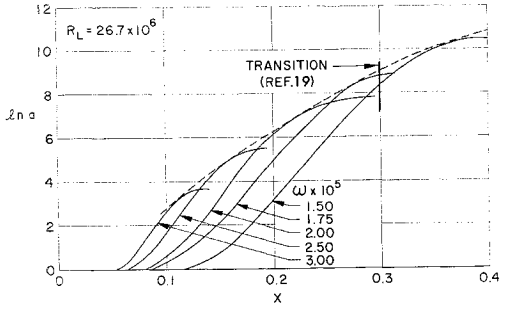

Fig. 9 Amplification factors—lower surface NACA 35-215, $C_L = 0.238$.

Reynolds numbers, R_L, of 25.0×10^6, 35.0×10^6, and 45.0×10^6. Figure 10 shows the observed location of transition X_{tr} (Ref. 20) as a function of R_L and theoretically predicted values based on a maximum amplification factor of e^{10}.

Amplification factors on a body of revolution of fineness ratio 9:1 (Ref. 21) were obtained at $R_L = 10.9 \times 10^6$, 6.65×10^6, and 5.2×10^6. The maximum amplification factors at transition for these Reynolds numbers are $e^{6.9}$, $e^{6.8}$, and $e^{7.9}$, respectively. A comparison between the experimental location of transition and the theoretical location based on an amplification factor of e^7 is shown in Fig. 11.

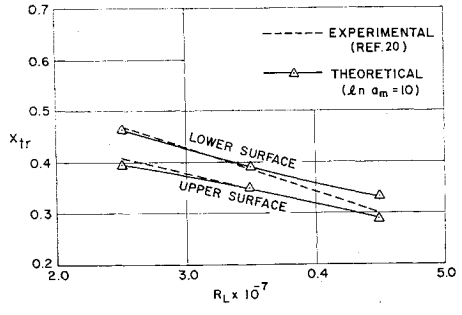

Fig. 10 Predicted and experimental location of transition—NACA $65_{(215)}$-114, $C_L = 0.14$.

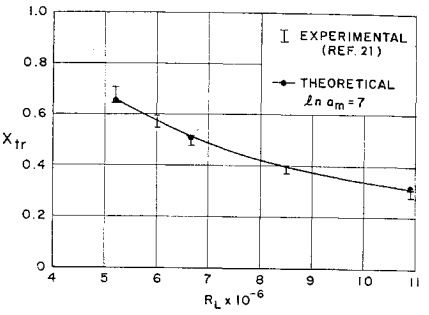

Fig. 11 Predicted and experimental location of transition—body of revolution. Fineness Ratio = 9 : 1.

Figure 12 shows a comparison between the experimental and theoretical location of transition over a range of freestream Reynolds numbers from 6.3×10^6 to 14.0×10^6 on a body of revolution of fineness ratio 10:1 (the experimental data was obtained from private communication with N. Gregory, NPL, England). The body is a paraboloid from the stagnation point up to $x = 0.35$, followed by a cylinder which extends downstream of the point of transition for the range of Reynolds numbers considered here. A good correlation between the experimental and theoretical location of transition is obtained for a constant maximum amplification factor of $e^{9.75}$.

It can be seen from Figs. 8, 10, 11, and 12 that good correlations between the experimental and theoretical location of transition can be obtained using a constant amplification factor. Generally speaking there is a tendency for the predicted location of transition to be low at the lower end of the Reynolds number range and high at the higher end of the Reynolds number range investigated for any particular body. For example, Fig. 8 shows that the predicted location of transition based on $a_m = e^{12}$ is slightly high at $R_L = 7.0 \times 10^6$. Similar behavior is noted for the other bodies investigated. One explanation offered is that as the freestream unit Reynolds number is increased the tunnel turbulence level increases and thus less total amplification is necessary to produce transition since the background disturbance amplitudes are larger to begin with.

Table 1 contains a summary of computed and experimental transition data. The data would seem to indicate that a good over-all correlation based upon a constant amplification factor can not be obtained due to the large variation of this quantity with the location of transition. However, it should be kept in mind that in attempting to predict transition a value of a_m is first chosen and what must be examined is the variation of the predicted transition location with amplification factor. Figure 13 shows the correlation obtained based on a maximum amplification factor of e^{10}. It is pointed out that high freestream turbulence levels and large amounts of surface roughness would tend to decrease a_m at transition. The over-all correlation, however, at least for two-dimensional bodies, is quite good.

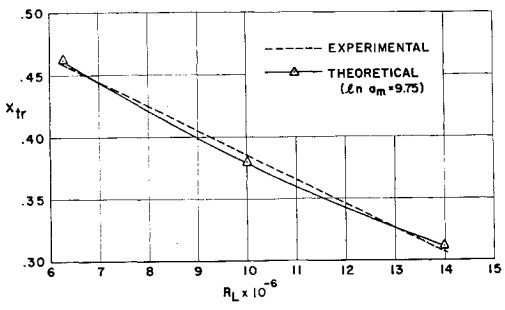

Fig. 12 Predicted and experimental location of transition—NPL body of revolution. F.R. = 10 : 1.

Table 1 Summary of transition data

$(u_\infty/\nu) \times 10^{-6}$ ft^{-1}	$R_L \times 10^{-6}$	$R_{x_{tr}} \times 10^{-6}$	X_{tr}	$\omega_{tr} \times 10^{5}$ [a]	ln a_m	Body	Comments	Ref.
		2.84		2.8	8.3	Flat plate	wind-tunnel test	2
		4.90		2.0	11.8		wind-tunnel reduced background noise	17
0.5	2.50	1.39	0.490	7.2	12.1	NACA 0012	$C_L = 0$; wind-tunnel test	18
1.0	5.00	2.08	0.355	5.2	10.6			
1.4	7.00	2.64	0.320	4.5	10.5			
1.57	26.7	15.4	0.453	1.5	9.9	NACA 35-215 top	$C_L = 0.238$; lower surface inferior,	19
1.57	26.7	9.0	0.299	1.7	9.0	NACA 35-215 bottom	flight test	
3.53	25.0	13.6	0.414	1.6	9.5	NACA $65_{(215)}$-114	$C_L = 0.14$; good	20
4.94	35.0	15.8	0.346	1.7	9.9	top	data, surface	
6.36	45.0	16.8	0.291	1.5	10.0		waviness begins at	
3.53	25.0	14.3	0.470	1.5	10.2	NACA $65_{(215)}$-114	$X = 0.37$, wind-	
4.94	35.0	16.4	0.385	1.4	9.7	bottom	tunnel test	
6.36	45.0	16.3	0.300	1.2	8.9			
1.36	10.9	3.35	0.28–0.31	4.5	6.9	Body of revolution F.R. = 9:1	wind-tunnel test	21
0.83	6.65	3.42	0.48–0.52	3.6	6.8			
0.65	5.20	3.74	0.69–0.72	3.0	7.9			
0.933	14.0	4.45	0.306	3.5	9.7	Body of revolution	wind-tunnel test	[b]
0.667	10.0	3.87	0.385	3.75	10.2	F.R. = 10:1		
0.420	6.3	2.91	0.458	4.0	9.5			

[a] Frequency producing maximum total amplification at transition, values accurate to within ±6%.
[b] Communicated by N. Gregory; NPL, England, 1955.

All the data with the exception of that for NACA 35-215 were obtained in wind tunnels. It is likely that the disturbance frequency-amplitude distribution characteristic of the particular tunnels had an effect on the results; hence, it is felt that a better correlation than that shown in Fig. 13 would be obtained using only free-flight test data. The present analysis could be modified to include the effect of the freestream disturbance frequency-amplitude distribution; however, the added complexities would greatly increase the effort necessary to predict transition.

The present results are encouraging in regard to the possibility of applying stability theory to the problem of predicting transition. In addition to including the effect of the freestream turbulence level, further refinements should take into account[14] the ratio of y velocity component fluctuation to x velocity component fluctuation and the Reynolds shear stress. It is pointed out that these quantities can also be obtained with the aid of stability theory, being directly related to the eigenfunctions satisfying the Orr-Sommerfeld equation.

One objection to the present analysis is that it is restricted to equations of motion in which the disturbances have been linearized. The success of such an approach will ultimately depend upon to what extend the transition region can be accurately represented by the linear theory. As of yet this question has not been answered and it is felt that the limitations of linear theory should first be fully explored before attempting the more difficult task of applying nonlinear theory.

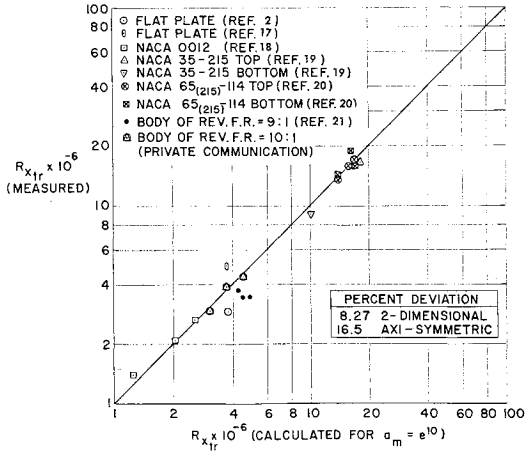

Fig. 13 Over-all correlation of transition data.

References

[1] Schlichting, H. and Ulrich, A., "On the Calculation of the Transition Laminar/Turbulent," *Jahrbuch*, 1942, d. DL I, p. 8.

[2] Schubauer, G. B. and Skramstad, H. K., "Laminar-Boundary-Layer Oscillations and Transition on a Flat Plate," Rept. 909, 1948, NACA.

[3] Bennett, H. W., "An Experimental Study of Boundary Layer Transition," Report prepared for the Office of Naval Research, Contract Nonr-673(00) Sept. 1953, Kimberly-Clark Corp.; also AD No. 18, 379, Armed Services Technical Information Agency.

[4] Smith, A. M. O., "Transition, Pressure Gradient, and Stability Theory," *Proceedings of 9th International Congress of Applied Mechanics*, Brussels, Belgium, Vol. 4, 1956, p. 234; also Rept. ES 26388, 1956, Douglas Aircraft Co., El Segundo, Calif.

[5] Van Ingen, J. L., "A Suggested Semiempirical Method for the Calculation of the Boundary-Layer Transition Region," Rept. V.T.H. 74, 1956, Dept. of Aeronautics and Engineering, Institute of Technology, Delft, Holland.

[6] Pretsch, J., "The Stability of a Two-Dimensional Laminar Flow in Pressure Drop and Pressure Rise," *Jahrbuch*, 1941, d. DL I, p. 58.

[7] Klebanoff, P. S., Tidstrom, D. K., and Sargent, L. M., "Boundary Layer Stabilization by Distributed Damping," *Journal of Fluid Mechanics*, Vol. 12, 1962, p. 1.

[8] Gaster, M., "A Note on the Relation Between Temporally Increasing and Spatially Increasing Disturbances in Hydrodynamic Stability," *Journal of Fluid Mechanics*, Vol. 14, 1962, p. 222.

[9] Landahl, M. T. and Kaplan, R. E., "The Effect of Compliant Walls on Boundary Layer Stability and Transition," AGARDograph 97, Pt. I, Naples, Italy, 1965.

[10] Bellman, R. E. and Kalaba, R. E., *Quasi-linearization and Nonlinear Boundary Value Problems*, American Elsevier, New York, 1965, pp. 98–103.

[11] Wazzan, A. R., Okamura, T. T., and Smith, A. M. O., "The Stability of Laminar Boundary Layers at Separation," *The Physics of Fluids*, Vol. 10, No. 12, 1967, p. 2540.

[12] Wazzan, A. R., Okamura, T. T., and Smith, A. M. O., "Spatial and Temporal Stability Charts for the Falkner-Skan Boundary-Layer Profiles," DAC 67086, Sept. 1, 1968, McDonnell Douglas Corp.

[13] Reshotko, E., "Stability Theory as a Guide to the Evalua-

tion of Transition Data," *Air Force Boundary Layer Transition Study Group Meeting*, Rept. BSD-TR-67, Vol. II, Sec. 13, Aug. 1967; AIAA Paper 68-669, Los Angeles, Calif., 1968.

[14] Liepmann, H. W., "Investigation of Boundary-Layer Transition on Concave Walls," ACR 4J28, Feb. 1945, NACA.

[15] Smith, A. M. O. and Clutter, D. W., "Solution of the Incompressible Laminar Boundary-Layer Equations," *AIAA Journal*, Vol. 3, No. 4, April 1963, pp. 639–647.

[16] Jaffe, N. A. and Okamura, T. T., "The Transverse Curvature Effect on the Incompressible Laminar Boundary Layer for Longitudinal Flow Over a Cylinder," *Zeitschrift fur Angewandte Mathematik und Physik*, Vol. 19, Fasc. 4, 1968, pp. 564–574.

[17] Wells, Jr., C. S., "Effects of Freestream Turbulence on Boundary-Layer Transition," *AIAA Journal*, Vol. 5, No. 1, Jan. 1967, p. 172.

[18] Von Doenhoff, A. E., "Investigation of the Boundary Layer About a Symmetrical Airfoil in a Wind Tunnel of Low Turbulence," Rept. L-507, Aug. 1940, NACA.

[19] Wetmore, J. W., Zalovcik, J. A., and Platt, R. C., "A Flight Investigation of the Boundary-Layer Characteristics and Profile Drag of the NACA 35-215 Laminar-Flow Airfoil at High Reynolds Numbers," Rept. L-532, May 1941, NACA.

[20] Braslow, A. L. and Visconte, F., "Investigation of Boundary-Layer Reynolds Number for Transition on a NACA $65_{(215)}$-114 Airfoil in the Langley Two-Dimensional Low-Turbulence Pressure Tunnel," TN 1704, Oct. 1948, NACA.

[21] Boltz, F. W., Kenyon, G. C., and Allen, C. Q., "Measurements of Boundary-Layer Transition at Low Speed on Two Bodies of Revolution in a Low Turbulence Tunnel," RM A56G17, 1956, NACA.

FEBRUARY 1970 AIAA JOURNAL VOL. 8, NO. 2

Hypersonic Similarity Solutions for Airfoils Supporting Exponential Shock Waves

J. D. Cole* and Jerome Aroesty†
The RAND Corporation, Santa Monica, Calif.

The flow behind concave and convex exponential shock waves is investigated from the viewpoint of inviscid, hypersonic small-disturbance theory. The supporting two-dimensional airfoil surfaces (which are in general not exponential) are determined, and the optimum such lifting surface, in terms of maximum $C_L^{3/2}/C_D$ for fixed C_D is shown to be only slightly more concave than a flat plate, and the improvement in performance over a flat plate is small. A limit line is shown to exist in the flowfield behind convex exponential shock waves, so that it is not possible to construct an airfoil that supports an exponential shock wave over its entire length if the nose curvature is too large. It is also indicated that this relatively refined theory must be used for studies of performance and optimization, since the results of Newtonian theory are only qualitatively applicable if γ is not unity.

Nomenclature

c^2 = $(\gamma - 1)/2\gamma$
C_L = $L/(\rho_\infty U^2/2)$, $C_D = D/(\rho_\infty U^2/2)$
D = drag
$F(x)$ = dimensionless body height
L = lift
P = pressure
p = dimensionless pressure [see Eq. (5)]
p^* = $(\gamma + 1)/2p$ [see Eq. (28)]
q = velocity
$S(x)$ = dimensionless shock height
U = freestream velocity
u,v = dimensionless velocity components
v^* = $(\gamma + 1)/2v$ [see Eq. (29)]
X = $x - \xi$ (distance from shock along streamline)
γ = specific heat ratio, C_p/C_V
δ = thickness ratio
θ = dimensionless shock slope
ξ = x location of streamline, where it crosses the shock wave
ρ = density
σ = density ratio [see Eq. (6)]
ψ = stream function

Received February 3, 1969; revision received July 17, 1969. This research is supported by the United States Air Force under Project RAND. Views or conclusions contained in this study should not be interpreted as representing the official opinion or policy of the United States Air Force.

* Consultant to The RAND Corporation.
† Engineer Environmental Sciences Dept., The RAND Corporation. Member AIAA.

I. Introduction

THE applications of hypersonic gas dynamics have in recent years been concerned with various aspects of reentry and missile phenomenology, whereas the development of criteria for the study and optimization of lifting and control surfaces has not been actively pursued. Because of this, there are few theoretical results relevant to the estimation of shock-wave/body interference phenomena and to the prediction of the effects of surface shape on control effectiveness in hypersonic flight. However, one well-known result, the "Newtonian chine strip," obtained using Newtonian gas dynamics, suggests that for a fixed drag penalty, surface concavity can result in an enhanced lift-to-drag ratio.

In the present paper this conjecture is subjected to a systematic investigation, in which the flowfield over a class of two-dimensional lifting surfaces (those which support exponential shock waves) is examined from the viewpoint of inviscid, hypersonic small-disturbance theory, and the effect of varying surface concavity on lift-to-drag ratio is then determined for fixed drag.

For $M_\infty = \infty$ and in the framework of inviscid, hypersonic small-disturbance theory, hypersonic similarity solutions with power law shocks and corresponding power law body shapes are well known.‡ In Ref. 3, it is indicated that a limiting case of similar flowfields with power law shocks is the flow-

‡ See Refs. 1 and 2 for a review of these results.